# Magnetic and magnetocaloric properties of $Ni_{47}Mn_{40}Sn_{13-x}Zn_x$ alloys: Direct measurements and first-principles calculations

A. Ghotbi Varzaneh,[1] P. Kameli,[1,*] I. Abdolhosseini Sarsari,[1] M. Ghorbani Zavareh,[2] C. Salazar Mejía,[2] T. Amiri,[3] Y. Skourski,[2] J. L. Luo,[3] T. H. Etsell,[3] and V. A. Chernenko[4,5]

[1]*Department of Physics, Isfahan University of Technology, Isfahan, 84156-83111, Iran*

[2]*Hochfeld-Magnetlabor Dresden (HLD-EMFL), Helmholtz-Zentrum Dresden-Rossendorf, 01328 Dresden, Germany*

[3]*Department of Chemical & Materials Engineering, University of Alberta, Edmonton, Alberta, Canada, T6G 1H9*

[4]*BCMaterials and University of Basque Country (UPV/EHU), Bilbao 48080, Spain*

[5]*Ikerbasque, Basque Foundation for Science, Bilbao 48013, Spain*

(Received 11 June 2019; accepted 12 March 2020; published 2 April 2020)

In the present study, the martensitic transformation (MT) and magnetic properties exhibited by the Ni-Mn-Sn Heusle-type magnetic shape memory alloys (MSMAs) doped with Zn have been investigated experimentally and theoretically. The inverse magnetocaloric effect (MCE) in $Ni_{47}Mn_{40}Sn_{13-x}Zn_x$ ($x = 0$, 1) was studied by direct measurements of the adiabatic temperature change, $\Delta T_{ad}$, in pulsed magnetic fields of 5, 10, and 20 T. The Zn doping of the Ni-Mn-Sn alloy led to a striking enhancement of the value of $\Delta T_{ad}$, e.g., from –2.5 for undoped to –11 K for Zn-doped alloys under a magnetic field amplitude of 20 T. The first-principles calculations were used to understand the origin of Zn-doping influence on MT, magnetic, and magnetocaloric properties. Particularly, the crystal structure and magnetic ordering influenced by the site occupancy in the undoped and Zn-doped alloys were analyzed. The results show that, whereas the usual transition metal elements with more valence electrons tend to enter the Ni sites, Zn atom prefers to occupy the Sn sublattice. The underlying physics of the drastic enhancement of MCE by Zn doping is discussed in terms of a partial disorder in the occupation sites of Zn atoms.

DOI: 10.1103/PhysRevB.101.134403

## I. INTRODUCTION

The Ni-Mn-based Heusler alloy systems are of great interest due to a wide variety of multifunctional properties that they exhibit owing to the martensitic transformation (MT) [1–3]. Particularly, magneto-, elasto-, and barocaloric effects in these materials have been a subject of the recent intense studies (see, e.g., [4–6] and references therein). As the result, these materials proved to be very promising candidates for application in the solid-state cooling systems (see [7]).

The Ni-Mn-based Heusler alloys exhibit a large magnetocaloric effect (MCE) due to the reversible magnetic-field-induced MT accompanied by a huge change of the magnetization. Generally, MCE can be characterized by the two main parameters: the magnetic-field-induced isothermal entropy change ($\Delta S_{iso}$) and the temperature change under adiabatic conditions of the applied magnetic field ($\Delta T_{ad}$). $\Delta S_{iso}$ is commonly considered to be correlated with the total entropy change $\Delta S_t$, accompanying the magnetic-field-induced first order MT, although recent theoretical studies did not confirm such a correlation directly [5]. $\Delta S_t$ is commonly described as a sum of the following contributions [8]:

$$\Delta S_t = \Delta S_{lat} + \Delta S_{mag} + \Delta S_{el}, \quad (1)$$

where $\Delta S_{lat}$, $\Delta S_{mag}$, and $\Delta S_{el}$ are the entropy changes related to the lattice, magnetic, and electronic subsystems. One should admit that Eq. (1) does not include a term related to the field-induced lattice deformation during MT [5], which is not important in the present work and can be disregarded. It has been experimentally demonstrated that the electronic contribution $\Delta S_{el}$ is negligibly small in Heusler alloys exhibiting MT near room temperature [9]. During MT, the superposition of $\Delta S_{mag} < 0$ and $\Delta S_{lat} > 0$ is usually assumed. Within this picture, the magnetic-field-induced reverse MT is accompanied by the positive changes in lattice entropy that dominates over the negative changes caused by the magnetic term leading to a negative adiabatic temperature change ($\Delta T_{ad} < 0$) termed an inverse MCE.

From the experimental point of view, the most studies on the inverse MCE, known from the literature, were performed by the calculations of $\Delta S_{iso}$ from the measured magnetization isotherms using the Maxwell equation [10]. On the other hand, taking into account possible applications, the direct measurement of $\Delta T_{ad}$ is the preferable and reliable technique to characterize a magnetocaloric response. The problem is that this method requires a homemade equipment, therefore the experimental data on $\Delta T_{ad}$ are still rather scarce in the literature. It is also desirable to measure $\Delta T_{ad}$ by using fast-sweeping magnets. The existing pulse-field facilities have the typical pulse lengths from 10 to 100 ms, which are close to the typical operational frequencies (10 to 100 Hz) of magnetocaloric cooling devices [11].

*kameli@cc.iut.ac.ir

 

It has to be noted that, unlike the slightly off-stoichiometric prototype $Ni_2MnGa$ ferromagnetic shape memory alloys (FSMAs), the Ni-Mn-$Z$ ($Z$ = In, Sn, and Sb) alloys undergo MT (and related functional properties) in the highly nonstoichiometric Mn-rich composition form $Ni_2Mn_{1+x}Z_{1-x}$, giving rise to the new class of MCE materials, the metamagnetic shape memory alloys (MetaMSMAs), which are characterized by the strong ferro-antiferromagnetic interactions between Mn atoms residing at different positions in the crystal lattice [12].

The crystal structure of the stoichiometric $X_2YZ$ Heusler alloys consist of four sublattice sites: A (0.25, 0.25, 0.25) and B (0.75, 0.75, 0.75) which are occupied by $X$, C (0, 0, 0) by $Y$, and D (0.5, 0.5, 0.5) by $Z$. In the nonstoichiometric case, the extra Mn atoms (Mn2) are located on the Sn sites. The magnetic moments of Mn2 atoms tend to be coupled antiferromagnetically (AFM) with the regular Mn atoms in the Mn sublattice (Mn1). The preferential Mn1 and Mn2 magnetic coupling changes with different $X$ (Ni, Co, Cu) [13] and $Z$ (In, Sn, Ga) [14–16] atoms. In some cases, the dopant (Co substitution for Ni) can change the stable magnetic configuration of the cubic phase [17]. Therefore, a change in magnetization during the forward MT is due to the change of the magnetic state (e.g., from FM to AFM) because MT is accompanied by the strong enhancement of AFM interactions resulting from the sharp decrease in the Mn-Mn distances [14,18,19].

A way to significantly improve MCE in Ni-Mn-$Z$ MetaMSMAs is to tailor the characteristics of MT and magnetic properties by adding a fourth element via partial substitution of $Z$, Ni, or Mn; this is being intensively investigated in the literature. Incorporation of 3$d$ transition metals (or other elements) in such alloys causes a strong influence on the electronic structure and the magnetic exchange interactions, leading to a rich interplay between crystal structure, magnetism, and electron conductivity across MT [20]. For example, an addition of Co and Cr to NiMn-based MetaMSMAs was perceived as an effective method to improve the magnetic properties [18]. It has to be noted that the site occupancy of the host and alloying atoms in the lattice is one of the fundamental issues towards understanding the alloying effect on the MCE properties [21]. In this regard, the first-principles methods should be ideal theoretical tools for the prediction of the magnetic and structural stability upon considering different site occupancy preferences and the magnetic configuration of the dopants.

In the present work, we systematically investigated, experimentally and theoretically, an influence of Zn doping on MT, magnetic and MCE properties exhibited by Ni-Mn-Sn MetaMSMA. Such a study is missing in the literature [7], which could be presumably explained by the difficulties of the alloy fabrication by standard melting techniques due to an easy vaporization of Zn. To avoid these difficulties, the $Ni_{47}Mn_{40}Sn_{13-x}Zn_x$ ($x$ = 0, 1) MetaMSMAs were prepared by the mechanical alloying. The $\Delta T_{ad}$ measurements under pulsed magnetic fields demonstrated that the Zn doping led to a multiple enhancement of the magnetocaloric response. Moreover, the MCE dynamics, in a desirable frequency range [22], was studied by checking the repeatability of MCE in a cyclic magnetic field. We also present the results of the first-principles calculations disclosing the equilibrium properties of crystal structure and magnetic ordering as a function of different site occupation of Zn. By comparing the results of these calculations with the experimental data, the nature of the improved magnetic properties and MCE of Zn-doped alloys was clarified.

## II. EXPERIMENTAL AND COMPUTATIONAL DETAILS

### A. Experimental methods

The $Ni_{47}Mn_{40}Sn_{13-x}Zn_x$ ($x$ = 0, 1) alloys were prepared by the mechanical alloying and heat-treated at 1223 K for 16 h according to the procedure described elsewhere [23]. The x-ray diffraction (XRD) patterns were collected using Cu K$\alpha$ radiation ($\lambda$ = 1.542 Å). The thermomagnetization, *M(T)*, measurements with the field-cooled-cooling (FCC), and field-cooled-heating (FCH) protocols were performed using a Quantum Design 9 T PPMS magnetometer under the applied magnetic fields of 0.1 and 5 T. The magnetization curves *M(H)* were recorded under magnetic fields up to 12 T using a vibration sample magnetometer (VSM) mounted in a Cryogenic Ltd. platform. Direct measurements of $\Delta T_{ad}$ have been done under pulsed magnetic fields with amplitudes of 5, 10, and 20 T using a home-built experimental setup at the Dresden High Magnetic Field Laboratory (HLD). The details of experimental setup and measuring procedures were described elsewhere [24]. The temperature change of the sample was monitored by a copper-constantan thermocouple glued between two plates of the alloy by a thermally conductive epoxy to optimize the thermal contact and reduce the heat losses. The total time for applying and removing pulse was 200 ms. A short pulse duration provided nearly adiabatic conditions and enabled investigation of the dynamics of MCE under realistic conditions of a refrigerating device. Despite the high field-sweep rate, the thermoelastic MT in MetaMSMAs is supposed to be fast enough to follow the magnetic field since the nucleation process and the phase boundaries movements should occur rapidly [11].

### B. Computational method

All computations were carried out using a plane-wave based density functional theory (DFT) implemented in the QUANTUM ESPRESSO package [25]. The projector augmented wave (PAW) pseudopotentials were employed with the following valence electron configurations: $4s^2 3d^8 4p^0$ for Ni, $3p^6 4s^2 3d^5$ for Mn, $5s^2 4d^{10} 5p^2$ for Sn, and $4s^2 3d^{10} 4p^0$ for Zn. All pseudopotentials were generated from PS library 0.3.1 employing the Perdew-Burke-Ernzerhof (PBE) exchange-correlation [26]. The nonstoichiometric compositions were treated by using the supercell approach. The calculations were done for the $Ni_8Mn_6Sn_2$ and $Ni_{16}Mn_{12}Sn_3Zn_1$ supercells containing 16 and 32 atoms, respectively, that were produced by VESTA [27]. The Broyden-Fletcher-Goldfard-Shanno (BFGS) algorithm with a convergence criterion of $10^2$ Ryd/Bohr was carried out to optimize lattice parameter of 16-atom supercell with $L2_1$ symmetry, and then repeating that in one direction two times we obtained 32-atoms supercell. We also considered two magnetic configurations in the lattice relaxation. The first one approximately corresponded to the $Ni_{47}Mn_{40}Sn_{13}$

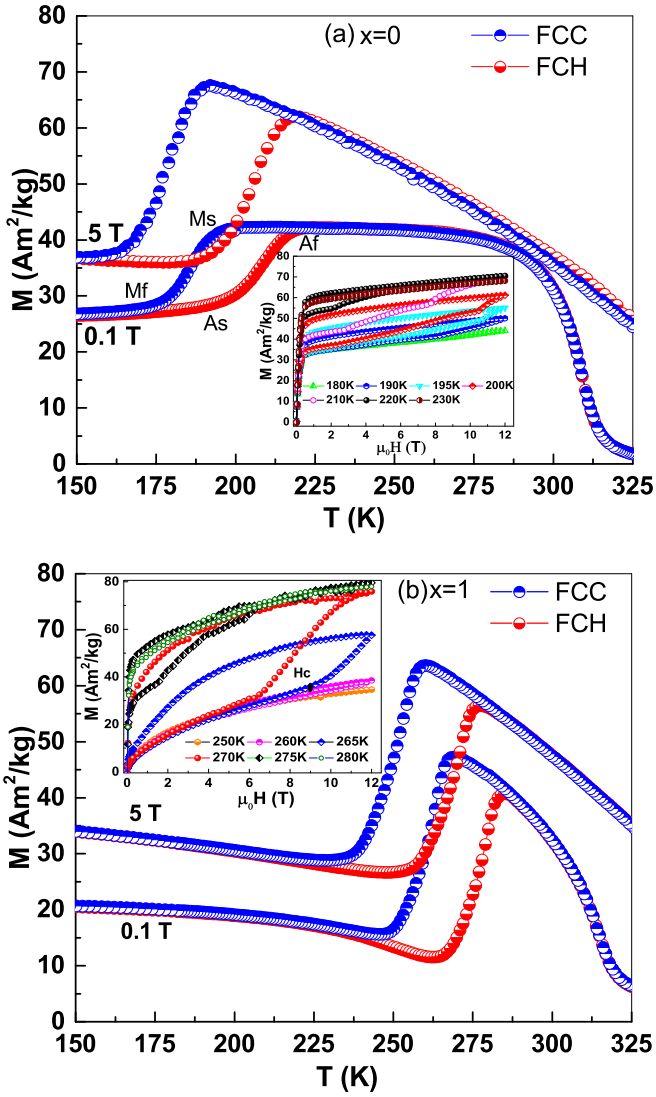


FIG. 1. Temperature dependencies of the magnetization *M(T)* for the $Ni_{47}Mn_{40}Sn_{13-x}Zn_x$ alloys with (a) $x = 0$ and (b) $x = 1$. The insets show *M(H)* curves at different temperatures around MT. $H_c$ is the critical value of magnetic field of the martensite-austenite start transformation at the selected temperature.

composition, and the second one to the $Ni_{47}Mn_{40}Sn_{12}Zn_1$. A kinetic energy cutoff of 450 eV was used for the plane-wave expansion. Test calculations with a larger number of $K$-points and higher values of the kinetic energy cutoff gave essentially the same results. The $K$-points for the 16 atoms supercell were always $8 \times 8 \times 8$, whereas the $8 \times 8 \times 4$ grid of $K$-points was used for the 32-atoms supercell.

## III. RESULTS AND DISCUSSION

### A. Transformation and magnetic properties

Figures 1(a) and 1(b) show the temperature dependencies of the magnetization *M(T)* for the $Ni_{47}Mn_{40}Sn_{13-x}Zn_x$ ($x = 0$ and 1) alloys under the applied field of 0.1 and 5 T, as typical examples. The martensite and austenite start and finish temperatures are denoted by $M_s$, $M_f$, $A_s$, and $A_f$, respectively. The ferromagnetic (FM) transition in the austenitic phase takes place at around $T_c^A \approx 313$ K and remains almost unchanged for both $x = 0$ and 1 alloys. $T_c^A$ appears rather insensitive to the changes in the Sn/Zn ratio. This observation suggests that the FM order is almost fully defined by the positive exchange interactions between the nearest neighbors of Mn in the regular sites, i.e., Mn1-Mn1 and Mn1-Ni, which are the same for both alloys [12,16].

Contrary to $T_c^A$, MT temperature strongly depends on Zn doping, e.g., $A_s \approx 195$ K for the Ni-Mn-Sn alloy and 260 K for the Zn-doped one. Such a behavior can be related to the increase of the valence electron concentration (e/a) (e.g., [28]). Also, a hybridization between Ni 3*d* and Mn 3*d* states could contribute to the enhancement of the MT temperatures [14,29–31]. In addition, with the decrease of Sn content, the relative quantity of Sn atoms contributing to the *p-d* hybridization between the main group element (Sn) and the transition metal element (Mn or Ni) decreases. As a result of all these factors, MT tends to occur at higher temperatures [31,32].

Upon increasing the magnetic field from 0.1 to 5 T, the austenitic phase is stabilized, and the MT temperature is linearly shifted to lower temperatures with the rates of –1.2 K/T for the Zn-free and –1.6 K/T for the Zn-doped samples. Taking into account a small difference in the transformation entropy change $\Delta S_t$, between these alloys, which can be inferred from the enough long distances of $M_s$ from $T_c^A$ in Fig. 1 (for details, see [33]), the higher shift in Zn-doped alloy, according to the Clausius-Clapeyron relationship, can be attributed to the larger magnetization difference ($\Delta M$) between the austenitic and martensitic phases observed in this alloy. The larger $\Delta M$ implies a higher Zeeman energy $\Delta M \times H$, consequently MT in this case is easier to be induced by a magnetic field [3,34]. The large values of both the magnetic-field-induced shift of MT and $\Delta M$ are prerequisites of a large MCE [8].

The insets to Fig. 1 depict the magnetization curves recorded up to 12 T at the constant temperatures in the vicinity of MT. Each *M(H)* measurement was performed according to the following protocol: after field ramp, the sample was reset in zero field to the austenitic phase by heating to 330 K, then cooled down to 100 K to complete the transformation into the martensitic phase, and, finally, heated up to the target temperature. The insets to Fig. 1 demonstrate that the magnetization gradually increases with magnetic field until the critical value $H_c$ is reached [indicated, as an example, for the curve at 265 K in the inset to Fig. 1(b)] then the metamagnetic-like hysteretic behavior proceeds, indicating a magnetic-field-induced transformation of some volume fraction of the martensite into the austenite. With increasing temperature, the critical field to induce MT decreases and a larger fraction of martensite transforms into the austenitic phase. By plotting a "$H_c$ versus T" phase diagram for both alloys (not shown), we found that the field-induced shift of the MT temperature is monotonously nonlinear (almost linear till 5 T), where the slope $dT/dH_c$, ranges from about –1.0 to –4.3 K/T at 0 and 12 T, respectively. The similar nonlinear temperature dependence of $H_c$ at high magnetic fields, typically observed for NiMn-based MetaMSMAs, has its origin in the phenomenon of thermal transformation arrest [35].

Finally, it can be seen that the magnetization of Zn-doped alloy is not saturated even at 12 T, which is attributed to a

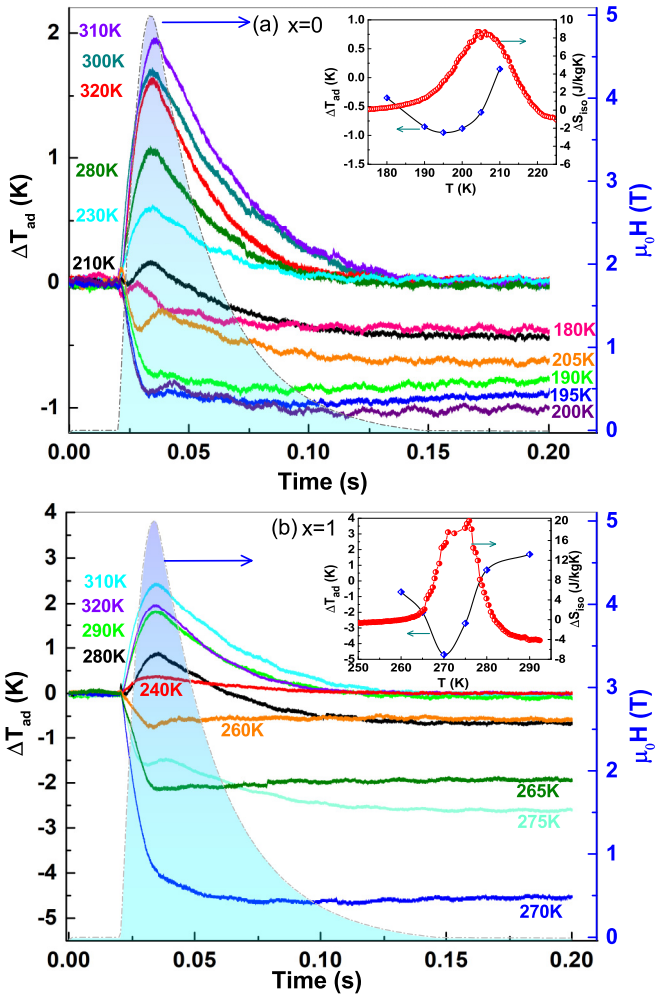


FIG. 2. Time dependencies of $\Delta T_{ad}$ (left axis) in the pulsed magnetic field of 5 T for (a) undoped and (b) Zn-doped alloys measured at different temperatures. The time dependencies of the magnetic field changes are also plotted. The insets show temperature dependencies of $\Delta T_{ad}$ maximums and $\Delta S_{iso}$ calculated from *M(T)* curves at different magnetic fields.

higher contribution of the antiferromagnetic coupling in this alloy [3].

### B. Magnetocaloric effect

The values of $\Delta T_{ad}$ under pulsed magnetic field of 5 T (rising time was 35 ms), measured in the range of both MT and ferromagnetic transition for the undoped and Zn-doped samples are depicted in Fig. 2. The pulsed field tests were conducted according to the same protocol as had been used for the *M(H)* measurements, whereby the sample was always in the complete martensitic state before heating it to the temperature at which the field application is done.

Figure 2 shows that whereas $\Delta T_{ad}$ value, equal to about +2 K at 5 T, for conventional MCE (produced by a spin ordering during the paramagnetic–ferromagnetic transition in austenite) does not depend of doping, this is not the case for the inverse MCE (produced by MT). As follows from Fig. 2, the maximum values of at the MT temperatures, equal to –0.9 K at 195 K for undoped and –4.7 K at 270 K for the Zn-doped samples, are obtained. A much larger value of $\Delta T_{ad}$ can be considered as an outstanding improvement of the inverse MCE response in the Zn-doped alloy. The same conclusion follows from the magnetic-field-induced entropy change $\Delta S_{iso}$, estimated at different temperatures by a standard Maxwell relationship using *M(T)* data at different magnetic fields (not shown). The peak values of $\Delta S_{iso}$ were obtained to be equal to 8.1 and 19.9 J/kg K for undoped and Zn-doped samples, respectively.

Note that MT in the doped alloy occurs near room temperature, which, in turn, is closer to $T_c^A$ than MT in the undoped one. With the MT temperatures approaching $T_c^A$, i.e., decreasing $(T_c^A - M_s)$, the contribution of the spin alignment (negative entropy change) decreases promoting the enlarged $\Delta T_{ad}$, what is observed in the Zn-doped alloy (see Sec. I and [9,36,37]). This enlargement is also reinforced by the higher value of $\Delta M$ between austenite and martensite and a stronger magnetic-field-induced shift of MT temperature in the Zn-doped alloy [38].

It is very interesting to point out that, contrary to the situation with conventional MCE, upon removing the magnetic field around MT, the samples still continue to cool further for some time instead of heating (Fig. 2). One obvious explanation of this anomaly could be related to the limited thermal conductivity and delay in the heat transfer from the sample to the temperature gauge, but other possible mechanisms could not be discarded as well. For example, as the magnetic field is reduced, at the first moments, the magnetic entropy changes related to the magnetic subsystem are dominant, leading to the conventional MCE, i.e., cooling. During further reduction of magnetic field the sample starts to transform into a martensite phase, causing an increased contribution from the transformation entropy, whereby the sample starts to warm up. These two processes can compensate, to some extent, each other causing a slow relaxation of $\Delta T_{ad}$.

It is well known that the thermal hysteresis of MT is the main issue influencing the cyclic behavior of the inverse MCE. This is also clearly demonstrated by the results shown in Fig. 3 . At the temperatures between $A_s$ and $A_f$ (205 and 280 K for $x = 0$ and $x = 1$, respectively) the samples are already partially transformed and the dependencies in Fig. 3 reflect that under a first pulse of the magnetic field, the alloys transform into complete (in undoped alloy) or into incomplete (in doped alloy) austenitic phase producing some $\Delta T_{ad}$ effect. The alloys keep the same state after field removal. Therefore, upon applying a second pulse, they exhibit only positive $\Delta T_{ad}$ due to a conventional MCE related to the ferromagnetic transition, as shown in Fig. 3.

The repeatability of the inverse MCE in three field-loading-unloading cycles has been checked for $x = 1$ sample at $A_s \approx 265$ K, when the sample is fully martensite. The inset to Fig. 3(b) displays the results for $\Delta T_{ad}(t)$ at the three subsequent pulses. It can be seen that subsequent magnetic field pulses lead to a gradual decrease of the inverse MCE due to a decrease of the volume fraction of the martensitic phase in the sample before each pulse. The first pulse induces a reverse MT, and the sample stays in the austenite phase. By reducing the field in the first pulse, some volume fraction of the sample remains in the austenite phase which does not

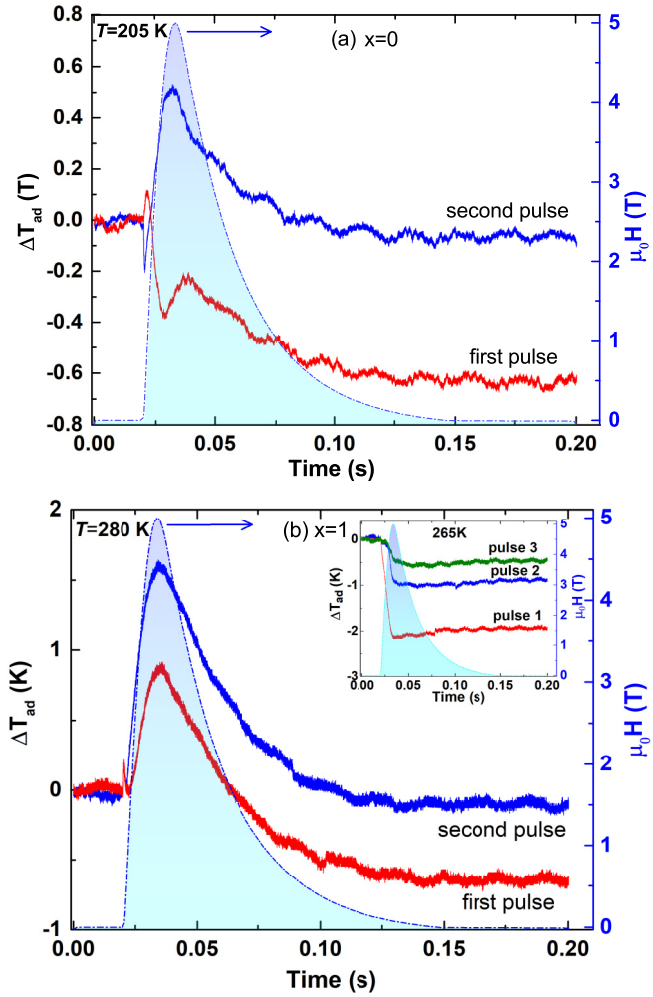


FIG. 3. Time dependencies of $\Delta T_{ad}$ under application of the first and second pulses of the magnetic field of 5 T for (a) $x = 0$ sample at 205 K and for (b) $x = 1$ sample at 280 K. The inset shows $\Delta T_{ad}(t)$ for the $x = 1$ alloy at 265 K under three subsequent pulses of magnetic field of 5 T.

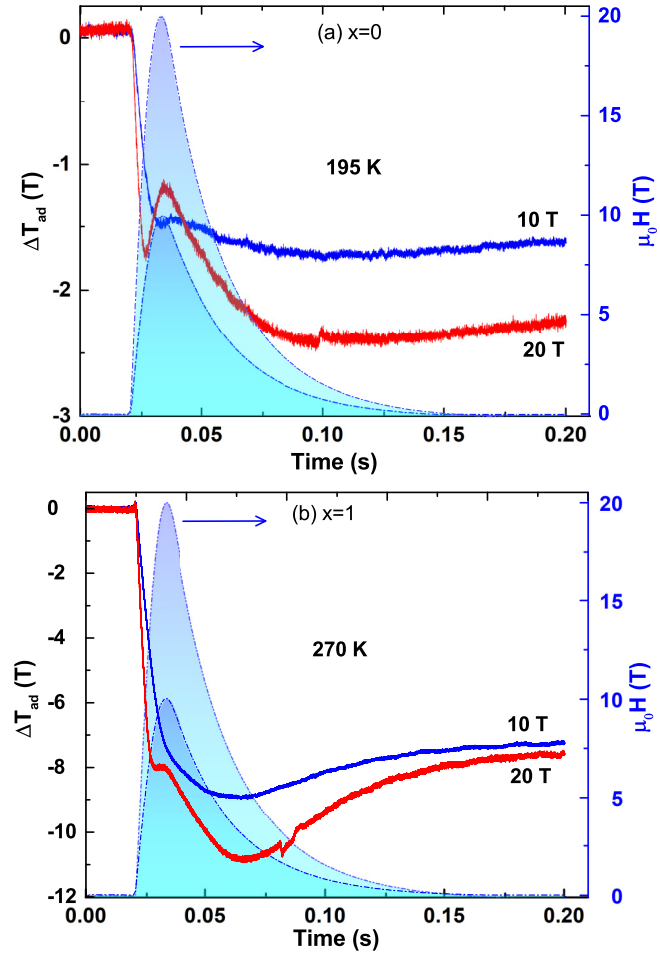


FIG. 4. Time dependence of $\Delta T_{ad}$ for (a) $x = 0$ and (b) $x = 1$ samples in the pulsed fields of 10 and 20 T.

transform back to martensite. Thus, the entropy changes due to the second and third pulses are becoming smaller and the maximum temperature change of the sample decreases. Such a poor cyclic behavior of $\Delta T_{ad}$ is due to a thermal hysteresis of MT [39], which is estimated from Fig. 1 to be equal to about 18 K. In the studied compound, a considerable MCE value was obtained under the first pulse of magnetic field. But to induce a repeatable MT and maintain large MCE value in a cyclic regime, one needs the higher magnetic fields or a combination of a magnetic field with an external mechanical force [40].

The maximum values of negative $\Delta T_{ad}$ (5 T) were observed at 195 and 270 K for $x = 0$ and $x = 1$ samples, respectively, see Fig. 2. So, these temperatures were selected for the experiments with the high-intensity pulsed magnetic fields of 10 and 20 T. Figure 4 reveals that the undoped sample exhibits $\Delta T_{ad}$= –1.8 K and –2.5 K for magnetic fields of 10 and 20 T, respectively, whereas the Zn-doped sample shows much larger values equal to –8.9 and –11 K for the same fields. This striking difference should be understood, at least qualitatively, by the theoretical considerations. In this sense, to provide the theoretical guide and gain a deeper insight into the role of Zn dopant in the transformation behavior, magnetism and inverse MCE, we carried out *ab initio* computations described in the next section.

### C. Computations

We performed *ab initio* calculations by the supercell approach. Using relaxation of atomic positions in the fixed unit cell volume equal to the ground state volume of the cubic structure, the total energy dependencies as a function of the tetragonality ratio $E(c/a)$ were obtained. Then, at the minimums of energies for selected values of $c/a$, the full relaxation, which included the atomic positions and unit cell lattice parameters, was carried out.

Figure 5(a) represents a 16-atoms supercell of $Ni_8Mn_6Sn_2$ with the schematically shown magnetic moments, which are coupled ferromagnetically (FM) when located in the Mn1-Mn1 and Ni-Mn1 positions, whereas the antiferromagnetic (AFM) interaction occurs between Mn1-Mn2. For the Zn-doped alloy, the supercell of $Ni_{16}Mn_{12}Sn_3Zn_1$ alloy was considered with 32 atoms [Fig. 5(b)]. In fact, for the doped alloy, at first, we used a big supercell with 64 atoms which

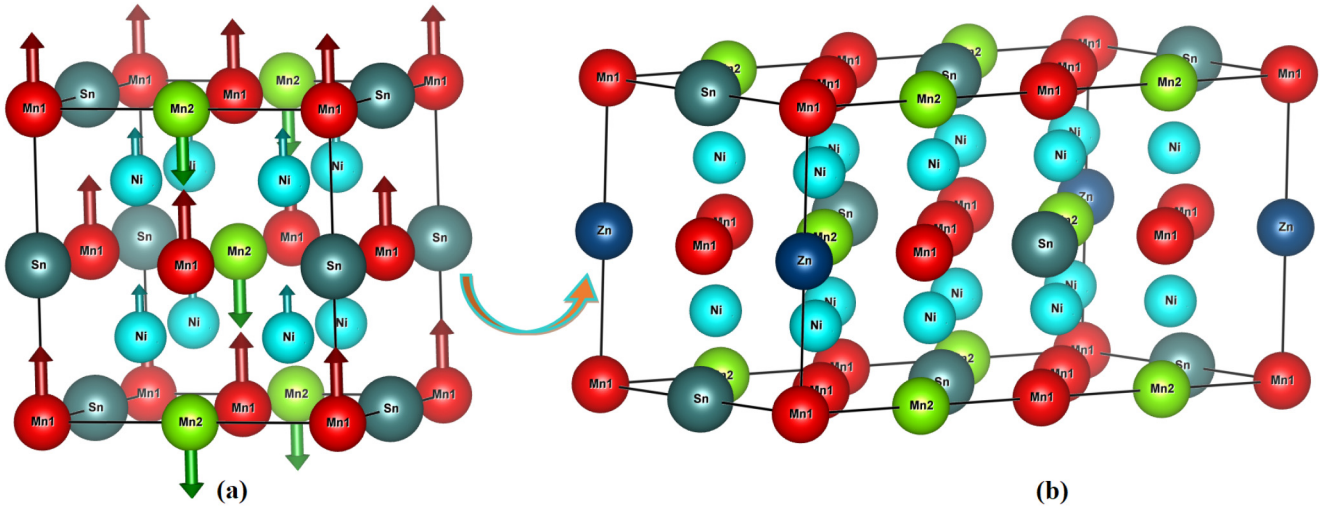


FIG. 5. (a) 16-atom supercell for $Ni_8Mn_6Sn_2$ Heusler-type alloy with mixed FM and AFM configuration of the magnetic moments; (b) 32-atom supercell of $Ni_{16}Mn_{12}Sn_3Zn_1$ alloy with the same magnetic configuration; magnetic moments are not shown to avoid overlapping. See Sec. I for the meaning of Mn1 and M2.

also fits its content, but the unit cell with 32 atoms provided almost the same results as bigger cell concerning the equilibrium lattice parameters and magnetic moments; therefore, the supercell with 32 atoms finally was used, essentially reducing computation time.

Table I presents the results of calculations of the lattice constants of the martensite and austenite, $c/a$ ratio and the values of magnetic moments for the FM and the AFM configurations together with the available experimental data. The results show that the AFM configuration of the cubic phase is more stable than FM for both undoped and Zn-doped alloys. According to the simulations, in the cubic structure of both undoped and Zn-doped alloys, the FM state is by 3.25 and 4.75 meV/atom less favorable than the AFM configuration. Comparing these differences, one can deduce that the FM interactions in the undoped sample are stronger than in the Zn-doped sample. For more direct evidence of this issue, the calculations of exchange parameters would be needed, which is beyond the scope of this paper. Note that the computation for some Ni-Mn-In and Ni-Co-Mn-Sn MetaMSMAs reveal that the FM configurations are more energetically favorable than AFM [14,41]. As already mentioned, the total magnetic configuration in MetaMSMAs is usually formed as a result of the competition between of Mn1-Mn2 AFM and Mn1-Mn1

TABLE I. Computed lattice parameters, total magnetization (also experimental), and partial magnetic moments for $Ni_8Mn_6Sn_2$ and $Ni_{16}Mn_{12}Sn_3Zn_1$ in the cubic and tetragonal phases. Different values of $c/a$ and magnetic configurations have been considered.

| Alloy | Lattice parameter (Å) | $\mu_{cal}^{Tot}$ ($\mu_B$/f.u.) | $\mu_{exp}^{Tot}$ ($\mu_B$/f.u.) | $\mu^{Ni}$ ($\mu_B$) | $\mu^{Mn1}$ ($\mu_B$) | $\mu^{Mn2}$ ($\mu_B$) | $\mu^{Sn}$ ($\mu_B$) | $\mu^{Zn}$ ($\mu_B$) |
|---|---|---|---|---|---|---|---|---|
| $Ni_8Mn_6Sn_2$(FM) | 5.983 | 6.47 | - | 0.54 | 3.48 | 3.52 | −0.03 | - |
| | 7.173 | | | | | | | |
| $Ni_8Mn_6Sn_2$(FM)($c/a = 1.312$) | | 6.44 | - | 0.59 | 3.40 | 3.49 | −0.05 | - |
| | 5.465 | | | | | | | |
| $Ni_8Mn_6Sn_2$(AFM) | 5.963 | 1.91 | - | 0.13 | 3.40 | –3.52 | –0.03 | - |
| | 7.069 | | | | | | | |
| $Ni_8Mn_6Sn_2$(AFM)($c/a = 1.314$) | | 1.62 | 1.98 | 0.07 | 3.16 | –3.30 | –0.05 | - |
| | 5.379 | | | | | | | |
| $Ni_{16}Mn_{12}Sn_{13}Zn_1$(FM) | 5.929 | 6.50 | - | 0.59 | 3.42 | 3.49 | –0.03 | –0.03 |
| | 7.159 | | | | | | | |
| $Ni_{16}Mn_{12}Sn_{13}Zn_1$(FM)($c/a = 1.327$) | | 6.29 | - | 0.58 | 3.38 | 3.44 | –0.05 | –0.04 |
| | 5.394 | | | | | | | |
| $Ni_{16}Mn_{12}Sn_{13}Zn_1$(AFM) | 5.909 | 1.98 | - | 0.18 | 3.31 | –3.42 | –0.03 | –0.02 |
| | 7.041 | | | | | | | |
| $Ni_{16}Mn_{12}Sn_{13}Zn_1$(AFM)($c/a = 1.319$) | | 1.73 | 1.66 | 0.12 | 3.15 | –3.28 | –0.05 | –0.03 |
| | 5.339 | | | | | | | |

and Ni-Mn1 FM exchange interactions, which strongly depend on lattice parameters, but also show a strong dependence on the conduction electrons of a $Z$ constituent in Ni-Mn-$Z$ ($Z$ = In, Sn, . . .) Heusler alloys [42,43].

Table I shows that the computed equilibrium lattice constant for AFM cubic phase is equal to 5.963 Å for undoped and 5.909 Å for Zn-doped alloys. A reduced value of the lattice parameter in Zn-doped alloy is explained by the smaller atomic radius of Zn (1.34 Å) compared to Sn (1.40 Å) [44]. It is worth noting, that the computed lattice parameters are in a reasonable agreement with the experimental ones (5.99 Å and 5.97 Å, respectively), that were measured by x-ray diffraction in the present work (not shown).

The total and individual magnetic moments for AFM and FM configurations were also calculated and they are listed in Table I. It can be seen that the Ni magnetic moment per site increases (from 0.13 to 0.18 $\mu_B$), indicating a stronger FM coupling with its neighboring atoms, whereas the magnetic moment on both Mn1 and Mn2 decreases with Zn substitution (cf. [45]). When the neighboring atoms are brought closer to each other, the interaction between them passes through the FM coupling with the maximum, after which FM is replaced by the AFM coupling for the reduced Mn-Mn interatomic distances [45]. An increase of the total moment is mainly related to the effect of the Ni moment. The magnetic moment of Ni shows a strong dependence on the $Z$ element [34]. In the Zn-doped alloy, with a reduction in the distance between Ni and Mn, the FM coupling between them are becoming stronger. This is in agreement with the calculated results for the magnetic moment of Ni in Ni-Mn-Sn alloys [45]. The magnetic moment per site in the Mn1 sublattice decreases (from 3.40 to 3.31 $\mu_B$), that may be due to the increased hybridization of the electronic states of the Ni and Mn atoms [46]. The magnetic moment of both Sn and Zn has a small AFM contribution in both the FM or AFM total configurations, which reflects the presence of Mn on the Sn sites. The small moments can be considered as a result of polarization of Sn and Zn atoms by the surrounding magnetically active atoms from the other crystallographic sites [8,47].

The Zn substitution increases the total magnetic moments from 1.91 $\mu_B$/f.u. for the undoped alloy to 1.98 $\mu_B$/f.u. for the Zn doped one. The increase in the total magnetic moment is in contrast with the experimental results. Such a discrepancy invokes a discussion about the role of the site occupancy of the alloying element which should affect both the electronic and the crystal structures and, hence, the magnetic behavior of the alloys. Generally, in $X_2YZ$ Heusler alloys, the site preference of $X$ and $Y$ transition metal atoms depends on the number of their valence electrons. Atoms with more valence electrons prefer the A and B positions, whereas the atoms with fewer valence electrons show a tendency to occupy the C position (see Sec. I for the sites notations). The main group element $Z$ enters into the D site [48]. Based on the so-called "valence electrons rule," the dopants of the transition metal elements with more valence electrons prefer entering Ni sites (A and B positions), while atoms with fewer valence electrons prefer entering the Mn1 site (C position) [49–51]. Therefore, one of the possible arrangements is that the Zn atoms occupy Ni or Mn sites, whereby driving some Ni or Mn atoms to the Sn sites. So, the difference between the calculated and experimental total magnetic moment in the present work can be attributed to the aforementioned possible occupations of Zn, as follows from the present first-principles analysis.

The first-principles calculations, indeed, were suitable to investigate an influence of the site occupancy of the doping element. For this purpose, a supercell with 32 atoms with the possibility of the occupation of Zn in different sites was considered. The relative total energy differences, $\Delta E'$, between four different possibilities of the occupation sites for Zn, compared to the state when Zn is located on Sn site, in the AFM magnetic configurations, their cubic lattice parameter and magnetic moment are listed in Table II . It has to be emphasized that, according to calculations, the AFM configuration was more stable than the FM one for all site occupancies.

The results indicate that Zn in the Sn site has lower total energy compared to Zn entering the Ni or Mn1 site. This result differs from other 3$d$ metals like Co. For example, in Co-doped alloys, regardless of the sublattice with the deficient component, the occupation of Co in the Ni site has the lowest energy among all possible configurations [21,51]. In contrast, our calculations show that in an ideal case of the fully equilibrium atomically ordered state of the Zn-doped alloy, Zn atoms occupy the Sn sublattice, which is also reinforced by the fact that Zn has entirely filled 3$d$ shell [49]. On the other hand, in a real material, which is out of global equilibrium, the Zn and Mn atoms on the Sn sites could be randomly distributed, moreover, Zn could occupy Ni and/or Mn sites, as well.

It is known that the atomic disorder in the Ni-Mn based Heusler MetaMSMAs can affect the electronic structure and the magnetic properties, as well as the MT temperature [52–55]. The computational study of these alloys has indicated that an additional degree of disorder between Mn and Sn atoms influences the magnetic properties, so the total magnetic moment can be reduced [15,56]. A similar situation can be assumed to happen in the present work (see Table II). A partial disorder due to the presence of Zn atoms on the Ni and Mn sites alongside the regular Sn sites (B2 and B32a structures [57]) is supported by the x-ray diffraction patterns shown in Fig. 6, where a reduction in the value of the "superlattice/main peak" intensity ratio is obtained for a Zn-doped alloy. The total energy of the occupation of Zn on Ni sites (see Table II) is close to the one when Zn occupies the Sn sites so, the intermixing of Zn on the Sn and Ni sublattices is highly possible causing a partial disorder. Therefore, an increasing amount of structural disorder, resulting in the perturbation of the magnetic exchange parameters, can cause a decrease in the saturation magnetization [15]. According to Table I, this decrease, although quite insignificant, is observed experimentally.

Furthermore, the mentioned partial atomic disorder can improve an inverse MCE in the Zn-doped alloy due to increase of the vibrational entropy change contribution at the transformation [58]. Thus, our results show that, the Zn-triggered atomic disorder can have an important impact on MCE in the present alloy system. The beneficial effect of Zn, compared to the Cu-doping, on the transformation behavior and magnetic anisotropy of martensite in the Ni-Mn-Ga FSMA was recently disclosed by the *ab initio* computations performed in [59].

TABLE II. The cubic lattice parameter, total magnetic moment, and relative total energy $\Delta E'$ (eV/f.u.) of different site occupancy in Zn-doped alloy with AFM configurations. $\Delta E'$ was obtained by extraction of the energy of the "normal" site occupation (Zn on Sn site), taken as a reference, from the total energy.

| Site occupancy of Zn in $Ni_{16}Mn_{12}Sn_3Zn_1$ | Schematic illustration | Lattice parameter Å | $\mu_{cal}^{Tot}$ ($\mu_B$/f.u.) | $\Delta E'$(eV/f.u.) AFM |
|---|---|---|---|---|
| $Ni_{16}Mn_{12}Sn_3Zn_1$ | Zn → Sn | 5.909 | 1.98 | 0 |
| | Zn → Ni | | | |
| $Ni_{15}Zn_1Mn_{12}Sn_3Ni_1$ | | 5.927 | 1.96 | 0.10 |
| | Ni → Sn | | | |
| | Zn → Mn | | | |
| $Ni_{16}Mn_{11}Zn_1Sn_3Mn_1$ | | 5.927 | 2.01 | 0.44 |
| | Mn → Sn | | | |
| | Zn → Mn, Mn → Ni | | | |
| $Ni_{15}Mn_1Mn_{11}Zn_1Sn_3Ni_1$ | | 5.921 | 1.74 | 0.60 |
| | Ni → Sn | | | |
| | Zn → Ni, Ni → Mn | | | |
| $Ni_{15}Zn_1Mn_{11}Ni_1Sn_3Mn_1$ | | 5.921 | 2.02 | 0.52 |
| | Mn → Sn | | | |

Now we consider electronic structure playing an important role in the underlying physics of the MT temperature increasing and the MCE improvement. To this end, the $t_{2g}$- and $e_g$-decomposed densities of states (DOS) of Ni 3*d* and Zn 3*d* were calculated in the equilibrium cubic phase with the AFM magnetic configuration and standard site occupancy. As can be seen in Figs. 7(a) and 7(b), the 3*d* states of Ni and the 3*d* states of Zn exhibit the bands mixing (spin hybridization). This is understandable since the Zn-Ni distance (2.635 Å) is lower than Zn-Mn distance (2.922 Å) in the equilibrium cubic structure; therefore, the covalent character of the bond between Ni and Zn is expected to be stronger than that between Mn and Zn [14,30,60]. In the Zn-doped alloy, the shifting and broadening of the total DOS could be caused by the hybridization of Zn-Ni and change in the hybridization of Ni 3*d* and Mn 3*d* orbitals [60,61]. With Zn doping, the peak (–0.09 eV) right below the Fermi level (in the minority of states), that has a sizable contribution near $E_F$, gets closer to the Fermi level position (–0.04 eV) [see Fig. 7(c)]. The increased overlapping with the Fermi level indicates a band Jahn-Teller-type of the instability of the corresponding cubic phase [62,63]. It explains an increase of the difference of energies between austenite and martensite, $\Delta E_{A\text{-}M}$, leading to the increase of MT temperature with a Zn doping. Some spin disorder caused by the hybridization of Zn with Ni, alongside a chemical disorder, should favor an enhancement of the magnetocaloric properties [64,65]. (The role of spin disorder in the functional properties of magnetocaloric materials, including MetaMSMAs, has also been discussed in [66–68]). Further studies explicitly revealing the spin exchange interactions are needed to confirm the effects of Zn.

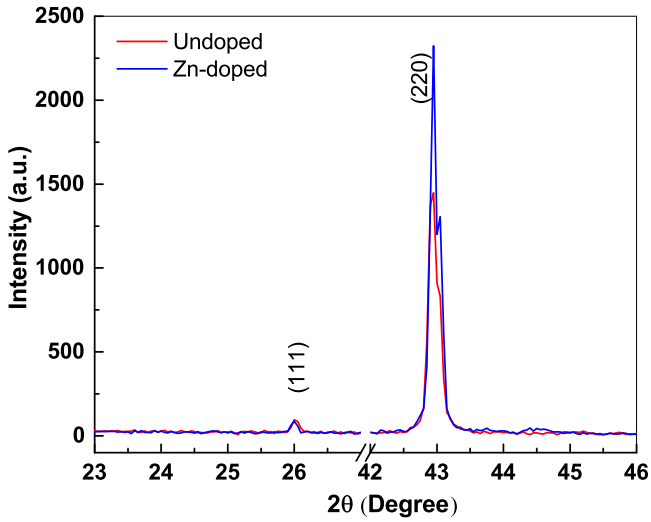


FIG. 6. X-ray diffraction patterns for undoped and Zn-doped alloys in the cubic phase to compare the intensities ratio between the superlattice and main peaks. For obviousness, the data were normalized to match intensities of the (111) reflections.

$\Delta E_{A\text{-}M}$ dependencies as a function of the tetragonal distortion $c/a$, computed in FM and AFM states, are shown in Fig. 8 . Figure 8 indicates that the AFM state is more stable for the entire range of $c/a$ ratios, which locally means that the Mn1-Mn2 magnetic interactions in both austenite and martensite are antiparallel. The ground state corresponds to a tetragonal structure with $c/a = 1.31$. The computed results show that $\Delta E_{A\text{-}M}$ effectively deepens with Zn doping. The larger $\Delta E_{A\text{-}M}$ corresponds to a higher MT temperature [19,30], which is in agreement with our experimental results. Computed results for both alloys show that MT is not accompanied by a change of magnetic configuration: AFM interaction between Mn1-Mn2 and FM interaction between Mn1-Mn1 and Mn1-Ni in both phase states and change in magnetization are due to a drastic change in the intensity of the AFM magnetic exchange interaction [18,69]. If the difference between the total energy of AFM and FM configurations is minimal (especially in the undoped sample), other factors might be considered as well. For example, as far as the DFT calculations are made at

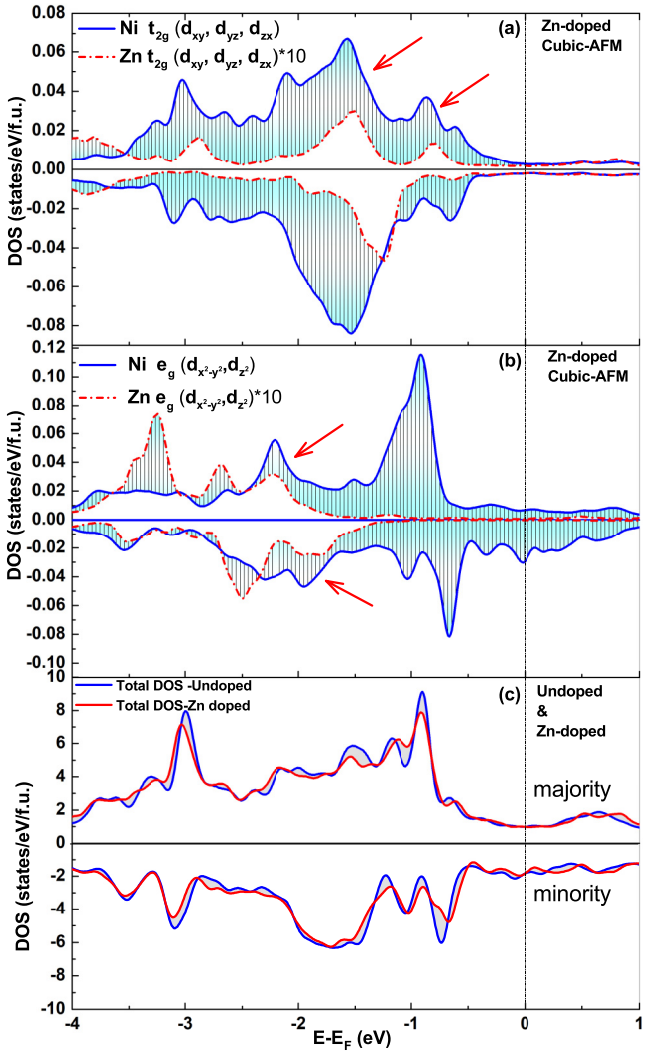


FIG. 7. The majority and minority-spin density of states (DOS) of Ni 3*d* and Zn 3*d* electrons in the equilibrium cubic phase. The Zn 3*d* DOS is multiplied by a factor of 10. The bands mixing (attributed to the spin hybridization) is indicated by the red arrows.

$T = 0$ K, an increase in temperature might change the energy of states considerably.

## IV. CONCLUSION

In the present work, the experimental and theoretical studies of the transformation behavior, magnetic properties, and inverse MCE of the $Ni_{47}Mn_{40}Sn_{13-x}Zn_x$ ($x = 0, 1$) MetaMSMAs were carried out. MCE was investigated by the direct measurements of $\Delta T_{ad}$ under pulsed magnetic fields. It was found that the addition of Zn to the ternary Ni-Mn-Sn alloy was an effective method for enhancing MCE response and enabling the MT temperature to be close to room temperature. Zn as a nonmagnetic dopant, not only increased the MT temperature to near room temperature, but also enhanced the maximum value of $\Delta T_{ad}$ by nearly a factor of 5. This was a remarkable result for MCE among the Ni-Mn-Sn MetaMSMAs, which makes this alloy system promising for applications.

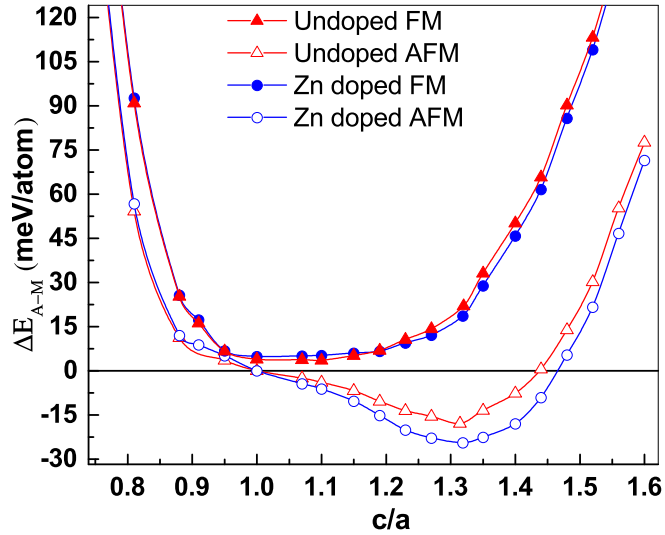


FIG. 8. Variation of the total energy as a function of tetragonal ratio $c/a$ for undoped and Zn-doped alloys with different magnetic configurations.

The structural and magnetic properties of these alloys were investigated in the framework of the DFT approach. Two different spin configurations of FM and AFM were considered. The calculations showed that the AFM configuration is more energetically favorable than FM for both the undoped and Zn-doped alloys in the entire range of $c/a$ ratios at 0 K, although the difference between FM and AFM states for the cubic phase is small. The last point therefore gives a real chance to further improvement in theory, which needs to be done since the experiment indicates the FM state for cubic phase.

As far as the site occupancy of the alloying elements affects the electronic and the crystal structures and the magnetic behavior of the alloys, its dependence on the Zn doping was analyzed by comparing the total energies of the alloy to different site occupancy configurations. The calculations demonstrated that in fully ordered structure, Zn atoms occupy the Sn sublattice.

The experimental results, in contrast to the computed ones, showed some reduction of the total magnetic moment with Zn doping that can be attributed to a partial disorder due to the occupation Ni and Mn sites by Zn atoms, instead of complete occupation of the regular Sn sites. The improvement of MCE in the Zn-doped alloy is attributed to an increase in the vibrational entropy change during MT related to a Zn-triggered partial disorder. Our results showed that this kind of disorder in the crystal lattice can have an important impact on MT, magnetic and MCE properties in the present alloy system.

From the electronic point of view, the DOS computations showed the possibility of hybridization of Zn 3*d* states with Ni 3*d* states, which might increase the spin disorder in the Zn-doped alloy leading to a larger inverse MCE, as observed experimentally.

Furthermore, the computations showed that the ground state for both alloys is a tetragonal structure with $c/a =$

1.31, indicating that the system is prone to undergo MT. The difference in the total energy of cubic and tetragonal phases, which controls the MT temperature, increases with increasing Zn content, in agreement with experimental results.

Our findings showed that an addition of the fourth component, such as, e.g., Zn, into ternary Ni-Mn-Sn alloys, causes interesting behavior worthy for basic studies. The results can be used to improve an inverse MCE and other functional properties not only in Ni-Mn-Sn alloys, but also in other Heusler-type MetaMSMAs.

## ACKNOWLEDGMENTS

We acknowledge the support of HLD at HZDR, a member of the European Magnetic Field Laboratory (EMFL). Funding from Spanish Ministry of Science and Innovations (Project No. RTI2018-094683-B-C53) is acknowledged. Technical and human support provided by the General Research Services of the UPV/EHU (SGIker) and, in particular, by I. Orue and A. Larrañaga, is appreciated. Computational resources are provided by Westgrid.

[1] R. Kainuma, Y. Imano, W. Ito, Y. Sutou, H. Morito, S. Okamoto, O. Kitakami, K. Oikawa, A. Fujita, T. Kanomata, and K. Ishida, Magnetic-field-induced shape recovery by reverse phase transformation, Nature **439**, 957 (2006).

[2] L. Mañosa, D. González-Alonso, A. Planes, E. Bonnot, M. Barrio, J.-L. Tamarit, S. Aksoy, and M. Acet, Giant solid-state barocaloric effect in the Ni-Mn-In magnetic shape-memory alloy, Nat. Mater. **9**, 478 (2010).

[3] P. Lázpita, M. Sasmaz, E. Cesari, J. Barandiarán, J. Gutiérrez, and V. Chernenko, Martensitic transformation and magnetic field induced effects in $Ni_{42}Co_8Mn_{39}Sn_{11}$ metamagnetic shape memory alloy, Acta Mater. **109**, 170 (2016).

[4] D. Salazar-Jaramillo, P. Álvarez-Alonso, P. Lázpita, J. S. Llamazares, P. Gorría, J. Blanco, and V. Chernenko, Magnetocaloric effect in specially designed materials, in *Magnetic Nanostructured Materials, Micro and Nano Technologies*, edited by A. A. El-Gendy, J. M. Barandiarán, and R. L. Hadimani (Elsevier, New York, 2018), Chap. 7, pp. 199–244.

[5] V. A. Chernenko, V. A. L'vov, E. Cesari, and J. M. Barandiarán, *Fundamentals of Magnetocaloric Effect in Magnetic Shape Memory Alloys*, edited by E. Brück, Handbook of Magnetic Materials Vol. 28 (Elsevier, New York, 2019), Chap. 1, pp. 1–45.

[6] E. Stern-Taulats, T. Castán, L. Mañosa, A. Planes, N. D. Mathur, and X. Moya, Multicaloric materials and effects, MRS Bull. **43**, 295 (2018).

[7] V. Franco, J. Blázquez, J. Ipus, J. Law, L. Moreno-Ramírez, and A. Conde, Magnetocaloric effect: From materials research to refrigeration devices, Prog. Mater. Sci. **93**, 112 (2018).

[8] T. Gottschall, K. P. Skokov, D. Benke, M. E. Gruner, and O. Gutfleisch, Contradictory role of the magnetic contribution in inverse magnetocaloric heusler materials, Phys. Rev. B **93**, 184431 (2016).

[9] T. Kihara, X. Xu, W. Ito, R. Kainuma, and M. Tokunaga, Direct measurements of inverse magnetocaloric effects in metamagnetic shape-memory alloy NiCoMnIn, Phys. Rev. B **90**, 214409 (2014).

[10] A. Smith, C. R. Bahl, R. Bjørk, K. Engelbrecht, K. K. Nielsen, and N. Pryds, Materials challenges for high performance magnetocaloric refrigeration devices, Adv. Ener. Mater. **2**, 1288 (2012).

[11] M. Ghorbani Zavareh, C. Salazar Mejía, A. K. Nayak, Y. Skourski, J. Wosnitza, C. Felser, and M. Nicklas, Direct measurements of the magnetocaloric effect in pulsed magnetic fields: The example of the heusler alloy $Ni_{50}Mn_{35}In_{15}$, Appl. Phys. Lett. **106**, 071904 (2015).

[12] V. D. Buchelnikov and V. V. Sokolovskiy, Magnetocaloric effect in Ni-Mn-X(X = Ga, In, Sn, Sb) heusler alloys, Phys. Met. Metallogr. **112**, 633 (2011).

[13] C.-M. Li, Q.-M. Hu, R. Yang, B. Johansson, and L. Vitos, Magnetic ordering and physical stability of $X_2Mn_{1+x}Sn_{1-x}$($X$ = Ru, Os, Co, Rh, Ni, Pd, Cu, and Ag) heusler alloys from a first-principles study, Phys. Rev. B **88**, 014109 (2013).

[14] C.-M. Li, H.-B. Luo, Q.-M. Hu, R. Yang, B. Johansson, and L. Vitos, Role of magnetic and atomic ordering in the martensitic transformation of Ni-Mn-In from a first-principles study, Phys. Rev. B **86**, 214205 (2012).

[15] V. V. Sokolovskiy, V. D. Buchelnikov, M. A. Zagrebin, P. Entel, S. Sahoo, and M. Ogura, First-principles investigation of chemical and structural disorder in magnetic $Ni_2Mn_{1+x}Sn_{1-x}$ heusler alloys, Phys. Rev. B **86**, 134418 (2012).

[16] V. D. Buchelnikov, V. V. Sokolovskiy, H. C. Herper, H. Ebert, M. E. Gruner, S. V. Taskaev, V. V. Khovaylo, A. Hucht, A. Dannenberg, M. Ogura, H. Akai, M. Acet, and P. Entel, First-principles and monte carlo study of magnetostructural transition and magnetocaloric properties of $Ni_{2+x}Mn_{1-x}Ga$, Phys. Rev. B **81**, 094411 (2010).

[17] V. Sokolovskiy, M. Zagrebin, and V. D. Buchelnikov, Magnetocaloric effect in Ni-Co-Mn-(Sn, Al) heusler alloys: Theoretical study, J. Magn. Magn. Mater. **459**, 295 (2018), the selected papers of Seventh Moscow International Symposium on Magnetism (MISM-2017).

[18] M. A. Zagrebin, V. V. Sokolovskiy, and V. D. Buchelnikov, *Ab initio* calculations of structural and magnetic properties of Ni-Co-Mn-Cr-Sn supercell, Intermetallics **87**, 55 (2017).

[19] X. Wang, J.-X. Shang, F.-H. Wang, C.-B. Jiang, and H.-B. Xu, Origin of unusual properties in the ferromagnetic heusler alloy Ni-Mn-Sn: A first-principles investigation, Scr. Mater. **89**, 33 (2014).

[20] K. P. Bhatti, S. El-Khatib, V. Srivastava, R. D. James, and C. Leighton, Small-angle neutron scattering study of magnetic ordering and inhomogeneity across the martensitic phase transformation in $Ni_{50-x}Co_xMn_{40}Sn_{10}$ alloys, Phys. Rev. B **85**, 134450 (2012).

[21] C.-M. Li, H.-B. Luo, Q.-M. Hu, R. Yang, B. Johansson, and L. Vitos, Site preference and elastic properties of Fe-, Co-, and Cu-doped $Ni_2MnGa$ shape memory alloys from first principles, Phys. Rev. B **84**, 024206 (2011).

[22] M. G. Zavareh, Y. Skourski, K. P. Skokov, D. Y. Karpenkov, L. Zvyagina, A. Waske, D. Haskel, M. Zhernenkov, J. Wosnitza, and O. Gutfleisch, Direct Measurement of the Magnetocaloric

Effect in La(Fe, Si, Co)$_{13}$ Compounds in Pulsed Magnetic Fields, Phys. Rev. Appl. **8**, 014037 (2017).

[23] A. Ghotbi Varzaneh, P. Kameli, V. R. Zahedi, F. Karimzadeh, and H. Salamati, Effect of heat treatment on martensitic transformation of $Ni_{47}Mn_{40}Sn_{13}$ ferromagnetic shape memory alloy prepared by mechanical alloying, Metals and Materials International **21**, 758 (2015).

[24] Y. Skourski, M. D. Kuzmin, K. P. Skokov, A. V. Andreev, and J. Wosnitza, High-field magnetization of $Ho_2Fe_{17}$, Phys. Rev. B **83**, 214420 (2011).

[25] P. Giannozzi, S. Baroni, N. Bonini, M. Calandra, R. Car, C. Cavazzoni, D. Ceresoli, G. L. Chiarotti, M. Cococcioni, I. Dabo, A. D. Corso, S. de Gironcoli, S. Fabris, G. Fratesi, R. Gebauer, U. Gerstmann, C. Gougoussis, A. Kokalj, M. Lazzeri, L. Martin-Samos, N. Marzari, F. Mauri, R. Mazzarello, S. Paolini, A. Pasquarello, L. Paulatto, C. Sbraccia, S. Scandolo, G. Sclauzero, A. P. Seitsonen, A. Smogunov, P. Umari, and R. M. Wentzcovitch, QUANTUM ESPRESSO: a modular and open-source software project for quantum simulations of materials, J. Phys.: Condens. Matter **21**, 395502 (2009).

[26] J. P. Perdew, K. Burke, and M. Ernzerhof, Generalized Gradient Approximation Made Simple, Phys. Rev. Lett. **77**, 3865 (1996).

[27] K. Momma and F. Izumi, *VESTA3* for three-dimensional visualization of crystal, volumetric and morphology data, J. Appl. Crystallogr. **44**, 1272 (2011).

[28] A. Çakır, M. Acet, and M. Farle, Exchange bias caused by field-induced spin reconfiguration in Ni-Mn-Sn, Phys. Rev. B **93**, 094411 (2016).

[29] S. R. Barman, S. Banik, and A. Chakrabarti, Structural and electronic properties of $Ni_2MnGa$, Phys. Rev. B **72**, 184410 (2005).

[30] C.-M. Li, H.-B. Luo, Q.-M. Hu, R. Yang, B. Johansson, and L. Vitos, First-principles investigation of the composition dependent properties of $Ni_{2+x}Mn_{1-x}Ga$ shape-memory alloys, Phys. Rev. B **82**, 024201 (2010).

[31] Z. Y. Wei, E. K. Liu, J. H. Chen, Y. Li, G. D. Liu, H. Z. Luo, X. K. Xi, H. W. Zhang, W. H. Wang, and G. H. Wu, Realization of multifunctional shape-memory ferromagnets in all-d-metal heusler phases, Appl. Phys. Lett. **107**, 022406 (2015).

[32] Y. Sutou, Y. Imano, N. Koeda, T. Omori, R. Kainuma, K. Ishida, and K. Oikawa, Magnetic and martensitic transformations of NiMnX (X = In, Sn, Sb) ferromagnetic shape memory alloys, Appl. Phys. Lett. **85**, 4358 (2004).

[33] J. M. Barandiarán, V. A. Chernenko, E. Cesari, D. Salas, P. Lázpita, J. Gutierréz, and I. Orue, Magnetic influence on the martensitic transformation entropy in Ni-Mn-In metamagnetic alloy, Appl. Phys. Lett. **102**, 071904 (2013).

[34] W. He, H. Huang, Z. Liu, and X. Ma, First-principles investigation of magnetic properties and metamagnetic transition of NiCoMnZ(Z = In, Sn, Sb) heusler alloys, Intermetallics **90**, 140 (2017).

[35] R. Y. Umetsu, X. Xu, and R. Kainuma, NiMn-based metamagnetic shape memory alloys, Scr. Mater. **116**, 1 (2016).

[36] C. Salazar Mejía, M. Ghorbani Zavareh, A. K. Nayak, Y. Skourski, J. Wosnitza, C. Felser, and M. Nicklas, Pulsed high-magnetic-field experiments: New insights into the magnetocaloric effect in Ni-Mn-In heusler alloys, J. Appl. Phys. **117**, 17E710 (2015).

[37] C. Aguilar-Ortiz, D. Soto-Parra, P. Álvarez-Alonso, P. Lázpita, D. Salazar, P. Castillo-Villa, H. Flores-Zúñiga, and V. Chernenko, Influence of Fe doping and magnetic field on martensitic transition in Ni-Mn-Sn melt-spun ribbons, Acta Mater. **107**, 9 (2016).

[38] D. R. Kumar, N. R. Rao, M. M. Raja, D. S. Rao, M. Srinivas, S. E. Muthu, S. Arumugam, and K. Suresh, Structure, magneto-structural transitions and magnetocaloric properties in $Ni_{50-x}Mn_{37+x}In_{13}$ melt spun ribbons, J. Magn. Magn. Mater. **324**, 26 (2012).

[39] T. Gottschall, K. P. Skokov, B. Frincu, and O. Gutfleisch, Large reversible magnetocaloric effect in Ni-Mn-In-Co, Appl. Phys. Lett. **106**, 021901 (2015).

[40] A. G. Gamzatov, A. M. Aliev, A. Ghotbi Varzaneh, P. Kameli, I. Abdolhosseini Sarsari, and S. C. Yu, Inverse-direct magnetocaloric effect crossover in $Ni_{47}Mn_{40}Sn_{12.5}Cu_{0.5}$ heusler alloy in cyclic magnetic fields, Appl. Phys. Lett. **113**, 172406 (2018).

[41] C.-M. Li, Q.-M. Hu, R. Yang, B. Johansson, and L. Vitos, Theoretical investigation of the magnetic and structural transitions of Ni-Co-Mn-Sn metamagnetic shape-memory alloys, Phys. Rev. B **92**, 024105 (2015).

[42] E. Şaşıoğlu, L. M. Sandratskii, and P. Bruno, Role of conduction electrons in mediating exchange interactions in Mn-based heusler alloys, Phys. Rev. B **77**, 064417 (2008).

[43] E. Şaşıoğlu, L. M. Sandratskii, and P. Bruno, Magnetic phase diagram of the semi-heusler alloys from first principles, Appl. Phys. Lett. **89**, 222508 (2006).

[44] A. G. Varzaneh, P. Kameli, T. Amiri, K. Ramachandran, A. Mar, I. A. Sarsari, J. Luo, T. Etsell, and H. Salamati, Effect of Cu substitution on magnetocaloric and critical behavior in $Ni_{47}Mn_{40}Sn_{13-x}Cu_x$ alloys, J. Alloys Compd. **708**, 34 (2017).

[45] X. Wang, J.-X. Shang, F.-H. Wang, C.-B. Jiang, and H.-B. Xu, Effect of 3d transition elements substitution for ni in $Ni_2Mn_{1+x}Sn_{1-x}$ on the phase stability and magnetic properties: A first principle investigation, J. Magn. Magn. Mater. **368**, 286 (2014).

[46] A. Chakrabarti, M. Siewert, T. Roy, K. Mondal, A. Banerjee, M. E. Gruner, and P. Entel, *Ab initio* studies of effect of copper substitution on the electronic and magnetic properties of $Ni_2MnGa$ and $Mn_2NiGa$, Phys. Rev. B **88**, 174116 (2013).

[47] H. C. Kandpal, G. H. Fecher, and C. Felser, Calculated electronic and magnetic properties of the half-metallic, transition metal based heusler compounds, J. Phys. D **40**, 1507 (2007).

[48] C. Xing, H. Zhang, K. Long, Y. Xiao, H. Zhang, Z. Qiu, D. He, X. Liu, Y. Zhang, and Y. Long, The effect of different atomic substitution at Mn site on magnetocaloric effect in $Ni_{50}Mn_{35}Co_2Sn_{13}$ alloy, Crystals **8**, 329 (2018).

[49] Z. Ni, X. Guo, Q. Li, Z. Liang, H. Luo, and F. Meng, Effect of Zn-doping on the phase transition and magnetic properties of heusler alloys $Ni_2MnGa_{1-x}Zn_x$ (x= 0, 0.25, 0.5, 0.75 and 1), J. Magn. Magn. Mater. **464**, 65 (2018).

[50] T. J. Burch, T. Litrenta, and J. I. Budnick, Hyperfine Studies of Site Occupation in Ternary Systems, Phys. Rev. Lett. **33**, 421 (1974).

[51] L. Ma, W. H. Wang, C. M. Zhen, D. L. Hou, X. D. Tang, E. K. Liu, and G. H. Wu, Polymorphic magnetization and local ferromagnetic structure in Co-doped $Mn_2NiGa$ alloys, Phys. Rev. B **84**, 224404 (2011).

[52] J. M. Barandiarán, V. A. Chernenko, E. Cesari, D. Salas, J. Gutiérrez, and P. Lázpita, Magnetic field and atomic order effect

on the martensitic transformation of a metamagnetic alloy, J. Phys.: Condens. Matter **25**, 484005 (2013).

[53] B. Weise, B. Dutta, N. Teichert, A. Hütten, T. Hickel, and A. Waske, Role of disorder when upscaling magnetocaloric Ni-Co-Mn-Al heusler alloys from thin films to ribbons, Sci. Rep. **8**, 9147 (2018).

[54] V. Sánchez-Alarcos, J. I. Pérez-Landazábal, V. Recarte, J. A. Rodríguez-Velamazán, and V. A. Chernenko, Effect of atomic order on the martensitic and magnetic transformations in Ni-Mn-Ga ferromagnetic shape memory alloys, J. Phys.: Condens. Matter **22**, 166001 (2010).

[55] N. Bruno, D. Salas, S. Wang, I. V. Roshchin, R. Santamarta, R. Arroyave, T. Duong, Y. Chumlyakov, and I. Karaman, On the microstructural origins of martensitic transformation arrest in a NiCoMnIn magnetic shape memory alloy, Acta Mater. **142**, 95 (2018).

[56] V. V. Sokolovskiy, M. A. Zagrebin, V. D. Buchelnikov, and P. Entel, The effect of anti-site disorder on structural and magnetic properties of Ni-Co-Mn-In alloys: *Ab initio* and monte carlo studies, IEEE Trans. Magn. **54**, 1 (2018).

[57] T. Graf, C. Felser, and S. S. Parkin, Simple rules for the understanding of heusler compounds, Prog. Solid State Chem. **39**, 1 (2011).

[58] V. Sánchez-Alarcos, J. López-García, I. Unzueta, J. Pérez-Landazábal, V. Recarte, J. Beato-López, J. García, F. Plazaola, and J. Rodríguez-Velamazán, Magnetocaloric effect enhancement driven by intrinsic defects in a $Ni_{45}Co_5Mn_{35}Sn_{15}$ alloy, J. Alloys Compd. **774**, 586 (2019).

[59] J. Janovec, L. Straka, A. Sozinov, O. Heczko, and M. Zelený, First-principles study of Zn-doping effects on phase stability and magnetic anisotropy of Ni-Mn-Ga alloys, Materials Research Express **7**, 026101 (2020).

[60] X. Wang, J.-X. Shang, F.-H. Wang, C.-B. Jiang, and H.-B. Xu, The structural stability and magnetic properties of the ferromagnetic heusler alloy Ni-Mn-Sn: A first principle investigation, J. Magn. Magn. Mater. **355**, 173 (2014).

[61] M. Ye, A. Kimura, Y. Miura, M. Shirai, Y. T. Cui, K. Shimada, H. Namatame, M. Taniguchi, S. Ueda, K. Kobayashi, R. Kainuma, T. Shishido, K. Fukushima, and T. Kanomata, Role of Electronic Structure in the Martensitic Phase Transition of $Ni_2Mn_{1+x}Sn_{1-x}$ Studied by Hard-X-Ray Photoelectron Spectroscopy and *Ab Initio* Calculation, Phys. Rev. Lett. **104**, 176401 (2010).

[62] Z. Liang, Q. Li, K. Sun, and H. Luo, Martensitic transition and magnetic structure in Zn-doped heusler alloy $Mn_2NiGa$: A theoretical approach, J. Phys. Chem. Solids **134**, 127 (2019).

[63] M. Zelený, A. Sozinov, L. Straka, T. Björkman, and R. M. Nieminen, First-principles study of Co- and Cu-doped $Ni_2MnGa$ along the tetragonal deformation path, Phys. Rev. B **89**, 184103 (2014).

[64] D. Comtesse, M. E. Gruner, M. Ogura, V. V. Sokolovskiy, V. D. Buchelnikov, A. Grünebohm, R. Arróyave, N. Singh, T. Gottschall, O. Gutfleisch, V. A. Chernenko, F. Albertini, S. Fähler, and P. Entel, First-principles calculation of the instability leading to giant inverse magnetocaloric effects, Phys. Rev. B **89**, 184403 (2014).

[65] V. D. Buchelnikov, V. V. Sokolovskiy, M. A. Zagrebin, M. A. Tufatullina, and P. Entel, First principles investigation of structural and magnetic properties of Ni-Co-Mn-In heusler alloys, J. Phys. D **48**, 164005 (2015).

[66] M. E. Gruner, W. Keune, B. Roldan Cuenya, C. Weis, J. Landers, S. I. Makarov, D. Klar, M. Y. Hu, E. E. Alp, J. Zhao, M. Krautz, O. Gutfleisch, and H. Wende, Element-Resolved Thermodynamics of Magnetocaloric $LaFe_{13-x}Si_x$, Phys. Rev. Lett. **114**, 057202 (2015).

[67] A. L. Wysocki, R. F. Sabirianov, M. van Schilfgaarde, and K. D. Belashchenko, First-principles analysis of spin-disorder resistivity of Fe and Ni, Phys. Rev. B **80**, 224423 (2009).

[68] J. Dubowik, K. Zaleski, I. Goscianska, H. Glowinski, and A. Ehresmann, Magnetoresistance and its relation to magnetization in $Ni_{50}Mn_{35}Sn_{15}$ shape-memory epitaxial films, Appl. Phys. Lett. **100**, 162403 (2012).

[69] V. V. Sokolovskiy, Y. A. Sokolovskaya, M. A. Zagrebin, V. D. Buchelnikov, and A. T. Zayak, Ternary diagrams of magnetic properties of Ni-Mn-Ga heusler alloys from *ab initio* and monte carlo studies, J. Magn. Magn. Mater. **470**, 64 (2019), International Baltic Conference on Magnetism: Focus on Functionalized Magnetic Structures for Energy and Biotechnology.